Ground-State Reverse Double Proton Transfer of 7-Azaindole

Pi-Tai Chou,*,† Wei-Shan Yu,† Youn-Chan Chen,† Ching-Yen Wei,† and Shannon Studer Martinez‡

Contribution from the Department of Chemistry, The National Chung-Cheng University, Chia-Yi, Taiwan, ROC, and Department of Chemistry and Biochemistry, College of Charleston, Charleston, South Carolina 29424

Received August 17, 1998

Abstract: Dynamics of the ground-state reverse proton transfer in 7-azaindole (7AI(N)) have been investigated by two-step laser-induced fluorescence (TSLIF) in various nonpolar solvents. Comprehensive analyses reveal a previously unrecognized finite rise kinetics for the long-lived transient species. Furthermore, the time-dependent spectral evolution indicates that the TSLIF spectrum obtained at the rise component is different from that of the decay component, while both spectra are red shifted relative to the prompt tautomer emission. The results lead us to propose that the transient species originates from the monomer of the 7AI proton-transfer tautomer (7AI(T)) produced by a minor dissociation channel (∼4%) of the excited 7AI(T) dimer, which subsequently undergoes a slow reverse proton transfer via the formation of a 7AI(T)/7AI(N) hydrogen-bonded complex. This proposed mechanism rationalizes the recent thermal lensing experiment which concluded that the 7AI(T) dimer is only 0.97 kcal/mol higher in energy than the 7AI(N) dimer,[35] while theoretical approaches,[38,39] in contrast, predict an energy difference of >20 kcal/mol.

Introduction

The spectroscopy and dynamics of 7-azaindole (7AI) have received considerable attention since the original observation of excited-state double proton transfer (ESDPT) by Taylor et al.[1] 7AI shows remarkable efficiency for the formation of the hydrogen-bonded complex with guest molecules possessing dual hydrogen-bonding sites. For example, the self-dimerization of 7AI with dual hydrogen bonds has long been recognized as a simplified model for the hydrogen-bonded base pair of DNA.[1−3] Spectroscopically, the change of UV−vis absorption spectra associated with the hydrogen-bonding formation has been used as a tool to obtain thermodynamics of the 7AI dimer. In a diluted solution with hydrocarbon solvents ($<10^{-5}$ M), monomer 7AI can be characterized by an S_0-S_1 absorption maximum at ∼285 nm. Upon increasing the concentration, the increase of absorbance at >310 nm is solely attributed to the 7AI dimer absorption, and a dimerization constant of $\sim 1.8 \times 10^3$ M^{-1} has been deduced in 3-methylpentane.[3] Upon excitation, it has been widely accepted that the excited-state double proton transfer (ESDPT) occurs through a self-catalysis or solvent (e.g., alcohols, acids) catalysis mechanism in 7AI hydrogen-bonded complexes.[4−26] For the case of 7AI dimer, the 310-nm excitation gives rise to an enormously large Stokes-shifted emission maximum at ∼480 nm which can be distinguished from the short-wavelength "normal" 7AI monomer fluorescence ($\lambda_{max} \sim$ 320 nm) in a very dilute hydrocarbon solution. Accordingly, the 480-nm emission is ascribed to the 7AI(T) dimer relaxation ($(7AI(T))^*_2 \rightarrow (7AI(T))_2$) resulting from the ESDPT reaction (see Figure 1; hereafter, (N) and (T) denote the normal and proton-transfer tautomer species, respectively).

In the jet-cooled isolated gas, Fuke et al. concluded that the ESDPT reaction on the 7AI(N) dimer was barrierless since it takes place from the zero vibrational level of the first excited state.[27,28] To elucidate the excited-state proton-transfer dynamics,

* To whom correspondence should be addressed.
† The National Chung-Cheng University.
‡ College of Charleston.

(1) Taylor, C. A.; El-Bayoumi, A. M.; Kasha, M. *Proc. Natl. Acad. Sci. U.S.A.* **1969**, *65*, 253.
(2) Ingham, K. C.; El-Bayoumi, M. A. *J. Am. Chem. Soc.* **1971**, *93*, 5023
(3) Ingham, K. C.; El-Bayoumi, M. A. *J. Am. Chem. Soc.* **1974**, *96*, 1674.
(4) Collins, S. T. *J. Phys. Chem.* **1983**, *87*, 3202.
(5) Bulska, H.; Grabowska, A.; Pakura, B.; Sepiol, J.; Waluk, J.; Wild, Urs, P. *J. Lumin.* **1984**, *29*, 65.
(6) McMorrow, D.; Aartsma, T. *Chem. Phys. Lett.* **1986**, *125*, 581.
(7) Tokumura, K.; Watanabe, Y.; Itoh, M. *J. Phys. Chem.* **1986**, *90*, 2362.
(8) Moog, R. S.; Bovino, S. C.; Simon, J. D. *J. Phys. Chem.* **1988,** *92*, 6545.
(9) Koijnenberg, J.; Huizer, A. H.; Varma, C. A. O. *J. Chem. Soc., Faraday Trans. 2* **1988**, *84* (8), 1163.
(10) Négreie, M.; Bellefeuille, S. M.; Whitham, S.; Petrich, J. W.; Thornburg, R. W. *J. Am. Chem. Soc.* **1990**, *112*, 7419.
(11) Moog, R. S.; Maroncelli, M. *J. Phys. Chem.* **1991**, *95*, 10359.
(12) Négrerie, M.; Gai, F.; Bellefeuille, S. M.; Petrich, J. W. *J. Phys. Chem.* **1991**, *95*, 8663.
(13) Chapman, C. F.; Maroncelli, M. *J. Phys. Chem.* **1992**, *96*, 8430.
(14) Chou, P. T.; Martinez, M. L.; Cooper, W. C.; McMorrow, D.; Collins, S. T.; Kasha, M. *J. Phys. Chem.* **1992**, *96*, 5203.
(15) Rich, R. L.; Negrerie, M.; Li, J.; Elliott, S.; Thronburg, R. W.; Petrich, J. W. *Photochem. Photobiol.* **1993**, *58*, 28.
(16) Negrerie, M.; Gai, F.; Lambry, J.-C.; Martin, J.-L.; Petrich, J. W. *J. Phys. Chem.* **1993**, *97*, 5046.
(17) Chen, Y.; Rich, R. L.; Gai, F.; Petrich, J. W. *J. Phys. Chem.* **1993**, *97*, 1770.
(18) Chen, Y.; Gai, F.; Petrich, J. W. *J. Am. Chem. Soc.* **1993**, *115*, 10158.
(19) Chen, Y.; Gai, F.; Petrich, J. W. J. *Phys. Chem.* **1994**, 98, 2203.
(20) Chen, Y.; Gai, F.; Petrich, J. W. *Chem. Phys. Lett.* **1994**, *222*, 329.
(21) Chang, C. P.; Hwang, W. C.; Kuo, M. S.; Chou, P. T.; Clements, J. H. *J. Phys. Chem.* **1994**, *98*, 8801.
(22) Chou, P. T.; Wei, C. Y.; Chang, C. P.; Chiu, C. H. *J. Am. Chem. Soc.* **1995**, *117*, 7259.
(23) Smirnov, A. V.; English, D. S.; Rich, R. L.; Lane, J. Teyton, L.; Schwabacher, A. W.; Luo, S.; Thornburg, R. W.; Petrich, J. W. *J. Phys. Chem.* **1997**, *101B*, 2758.
(24) Takeuchi, S.; Tahara, T. *Chem. Phys. Lett.* **1997**, 277, 340.
(25) Lopez-Martens, R.; Long, P.; Solgadi, D.; Soep, B.; Syage, J.; Millie, Ph. *Chem. Phys. Lett.* **1997**, *273*, 219.
(26) Nakajima, A.; Hirano, M.; Hasumi, R.; Kaya, K.; Watanabe, H.; Carter, c. C.; Williamson, J. M.; Miller, T. A. *J. Phys. Chem. A* **1997**, *101*, 392.

10.1021/ja982940d CCC: $15.00
Published on Web 12/01/1998

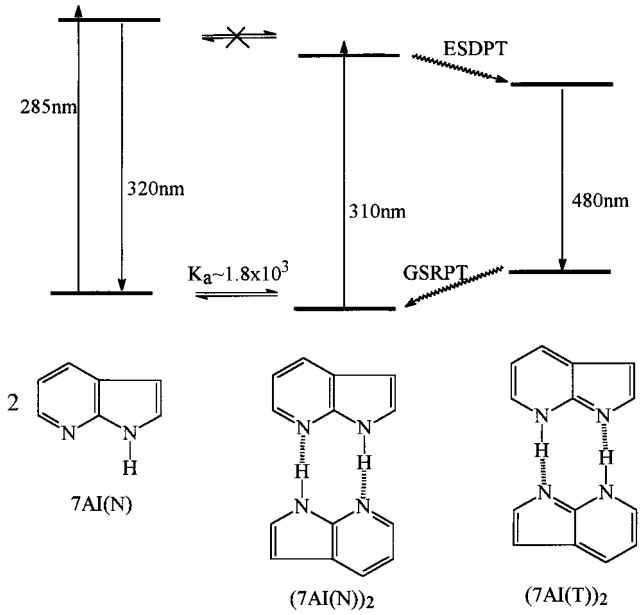

Figure 1. Photophysics of 7AI and 7AI dimer in hydrocarbon solvents (only depicting singlet-state manifolds). Note that an equilibrium between excited 7AI and 7AI dimer is not established due to the fast S_1-S_0 relaxation and ESDPT for 7AI and 7AI dimer, respectively.

ultrafast time-resolved measurements have been carried out. Recently, Zewail et al.[29] applied femtosecond mass spectroscopy to investigate the reaction dynamics of the 7AI(N) dimer in an isolated gas system and concluded that the ESDPT takes place through a sequential, two-step proton-transfer process in which the overall reaction time, depending on the excitation frequency, proceeds within 3 ps. In the condensed phase, pico-femtosecond studies have revealed that the rate of proton transfer is within 0.3×10^{12} to 1×10^{12} s^{-1} for the case of the 7AI(N) dimer in nonpolar solvents.[30,31] Very recently, on the basis of an improved femtosecond technique, Chachisvillis et al.[32] have further resolved the details associated with the ESDPT of the 7AI(N) dimer in various solvents and concluded that on the global potential energy surface both trajectories of the symmetric and asymmetric vibrational motion must be considered for the proton-transfer reaction.

In contrast, the rate of ground-state reverse proton transfer (GSRPT) for the 7AI(T) dimer has been reported to be surprisingly slow. By applying transient absorption and two-step laser-induced fluorescence (TSLIF) measurements, Itoh et al. demonstrated that an unexpectedly long-lived (~microseconds) 7AI(T) dimer is involved in the GSRPT at room temperature.[33,34] Very recently, on the basis of a time-resolved thermal lensing technique, Suzuki et al.[35] observed a slow-rising thermal lensing signal of which the relaxation dynamics are, in part, in agreement with those obtained by Itoh et al. (vide infra), confirming the existence of the long-lived tautomer species. Taking advantage of the fact that the thermal lensing technique essentially measures the heat dissipation upon the radiationless transition, Suzuki et al. were able to extract the enthalpy factor for the 7AI(T) dimer → 7AI(N) dimer reverse proton-transfer reaction. Consequently, a surprisingly small ΔH value of 0.97 kcal/mol was deduced, which is in general much smaller than other molecules exhibiting a proton-transfer reaction. For example, the enthalpy change of keto−enol tautomerism for 7-hydroxyquinoline in methanol was reported to be 9.76 kcal/mol.[36] For the case of 2-methylbenzophenone, the enthalpy of formation was obtained to be 27.6 kcal/mol for cis-enol and 48.0 kcal/mol for trans-enol.[37] As for the 7AI dimer, ΔH for the 7AI(N) dimer → 7AI(T) dimer tautomerism in the ground state has been theoretically calculated to be 24.5 and 22.3 kcal/mol using 4-31G[38] and 6-31G*[39] basis sets, respectively, which are apparently much larger than the experimental value of 0.97 kcal/mol. In this study, we have also performed a calculation based on a more advanced CBS-4 method,[40] and the results show the enthalpy difference between the 7AI(N) and 7AI(T) dimer to be 23.5 kcal/mol.[41] Therefore, ΔH obtained from the thermal lensing experiment is generally ~20 kcal/mol less than that predicted from theoretical approaches. Such a surprising difference has been tentatively explained by a drastic conformational change between the normal and tautomer forms and/or the solvation effect of surrounding molecules.[35] However, this proposed mechanism cannot be rationalized, at least, by ab initio calculations in the gas phase, unless solvation plays a major role to account for a significant structural distortion, hence stabilizing the 7AI(T) dimer. To further verify this viewpoint, we have performed a semiempirical calculation based on the PM3-SM3 model,[42] and the results predict similar solvation energies between the 7AI(N) and 7AI(T) dimers in *n*-heptane solution, indicating that a structural change due to the induced-dipole interaction in nonploar solvents is negligible.

To resolve this controversy, we have therefore reinvestigated the GSRPT of the 7AI(T) dimer by an ultrasensitive nanosecond pump−probe TSLIF technique. This system is based on an intensified charge-coupled detector so that both time and spectral evolution can be acquired simultaneously, giving more dimensions for spectral and dynamic analyses. The results lead us to conclude that the transient species may originate from the 7AI(T) monomer generated by the dissociation of the 7AI(T) dimer during its excited-state life span. Subsequently, a slow GSRPT takes place through the formation of a 7AI(T)/7AI(N) hydrogen-bonded complex.

Experimental Section

Materials. 7AI (Aldrich) was twice purified by column chromatography where 1:1 (v/v) *n*-hexane:ethyl acetate was used as an eluent. A conventional method by saturating 7AI in ethanol or *n*-heptane at

(27) Fuke, K.; Yoshiuchi, H.; Kaya, K. *J. Phys. Chem.* **1984**, *88*, 5840.
(28) Fuke, K.; Kaya, K. *J. Phys. Chem.* **1989**, *93*, 614.
(29) Douhal, A.; Kim, S. K.; Zewail, A. H. *Nature* **1995**, *378*, 260.
(30) Hetherington, W. M., III; Micheels. R. H.; Eisenthal, K. B. *Chem. Phys. Lett.* **1979**, *66*, 230.
(31) Share, P. E.; Sarisky, M. J.; Pereira, M. A.; Repinec, S. T.; Hochstresser, R. M. *J. Lumin.* **1991**, *48/49*, 204.
(32) Chachisvillis, M.; Fiebig, T.; Douhal, A.; Zewail, A. H. *J. Phys. Chem. A.* **1998**, *102*, 669.
(33) Tokumura, K.; Watanabe, Y.; Itoh, M. *J. Chem. Phys. Lett.* **1986**, *90*, 2362.
(34) Tokumura, K.; Watanabe, Y.; Udagawa, M.; Itoh, M. *J. Am. Chem. Soc.* **1987**, *109*, 1346.
(35) Suzuki, T.; Okuyama, U.; Ichimura, T. *J. Phys. Chem. A* **1997**, *101*, 7047.
(36) Terazima, M.; Azumi, T. *J. Am. Chem. Soc.* **1989**, *111*, 3824.
(37) Suzuki, T.; Okuyama, U.; Ichimura, T. *Chem. Phys. Lett.* **1997**, *266*, 107.
(38) Douhal, A.; Guallar, V.; Moreno, M.; Lluch, J. M. *Chem. Phys. Lett.* **1996**, *256*, 370.
(39) Chou, P. T.; Wei, C. Y.; Chang, C. P.; Kuo, M. S. *J. Phys. Chem.* **1995**, *99*, 11994.
(40) Uchterski, J. W.; Petersson, G. A.; Montgomery, J. A., Jr. *J. Chem. Phys.* **1996**, *104*, 2598. See Theoretical Calculation for a detailed description.
(41) On the basis of the CBS-4 method, the difference between the heat of formation of 7AI monomer and that of its tautomer, 7AI(T), was calculated to be 14.48 kcal/mol.
(42) A PM3-SM3 method developed by Cramer and Truhlar[43] was applied to calculate the solvation free energy. The solvation free energies were obtained with an AMSOL version 5.4 program[44] and then added to "gas-phase" energies obtained from the ab initio method. This combination method has proven to reproduce the experimental results, especially the relative stabilization energy of various proton-transfer tautomers, reasonably well.

the boiling temperature followed by recrystallization is not recommended due to certain degrees of thermal decomposition, giving rise to a reaction product with strong fluorescence interference (vide infra). The purity of 7AI was checked by the fluorescence excitation spectrum in cyclohexane under sufficiently low concentration of $<10^{-6}$ M, where the 7AI monomer form exists predominantly. N(1)-deuterated 7AI was prepared by dissolving 7AI in O′-deuterated ethyl alcohol (TCI, 99.5%) and stirring for 1 h and subsequently vacuum evaporation. This procedure was repeated three times to obtain deuterated 7AI, which was then stored in a drybox for later use. Hydrocarbon solvents from *n*-heptane to hexadecane were all of spectragrade (Aldrich) and used right after received. Acetic acid (Merck Inc.) was purified through a fractional distillation.

Measurements. Steady-state absorption and emission spectra were recorded by a Cary 3E (Perkin-Elmer) spectrophotometer and a Hitachi (SF4500) fluorimeter, respectively. The excitation light source of the fluorimeter has been corrected by the Rhodamine B spectrum. In addition, the wavelength-dependent characteristics of the monochromator and photomultiplier have been calibrated by recording the scattered light spectrum of the corrected excitation light from a diffused cell in the range 220−700 nm. Lifetime studies were performed by an Edinburgh FL 900 photon counting system with a hydrogen-filled flash lamp or a nitrogen lamp as the excitation source. The temporal resolution after deconvolution of the excitation pulse was 200 ps. The data were analyzed using a nonlinear least-squares fitting program with a deconvolution method reported previously.[45]

For the TSLIF experiment, a Nd:YAG (355 nm, 5 ns, Continuum Surlite II) pumped optical parametric oscillator (OPO) was tuned to 620 nm, which was then frequency doubled by a BBO crystal (10 mm path length) to obtain a 310-nm excitation frequency for the pump pulse. As mentioned in the Introduction only 7AI(N) dimer is excited upon 310-nm excitation, resulting in the ESDPT. Conversely, another Nd:YAG laser (Continuum Surlite II) with third-harmonic generation (355 nm, 5 ns) was used as a probe pulse. It has been shown in the transient absorption study that the long-lived proton-transfer tautomer species exhibits an S_0-S_1 absorption band maximum at ∼350 nm.[33,34] Both pump and probe lasers are externally controlled by a programmable delay pulse generator (SRS Model DG-535) which also triggers a high-voltage pulse amplifier (Princeton Instrument, PG-200) to gate the intensified charge coupled detector (ICCD, Princeton Instrument, Model 576G/1). The actual time delay between two pulses was monitored by a photodiode (EG&G model FND-100) and recorded by a 2.5-GHz bandwidth transient digitizer (Lecroy 9360). Both pump and probe pulses were projected across the flowing sample at 180° with beam diameters of 3.5 and 3.0 mm, respectively. The resulting fluorescence was focused by a camera lens (Nikon $f^{\#} = 1.0$) to the entrance slit of a monochromator (Acton, SpectraPro-500) and detected by an ICCD. To eliminate the scattering light of the probe pulse a 355-nm holographic filter (Kaiser Optical Systems, Inc.) was placed in front of the entrance slit. In the laser-power-dependent study of TSLIF, the intensity of both pump and probe laser pulses was tuned by a half-wave plate (CVI) in combination with a Glan-Laser polarizer (Lambda Research Optics Inc.). Laser pulse energies were measured by a power meter (Moletron PM-500D). Low-energy pulses (100 μJ to 1.0 mJ) were applied for both pump and probe lasers to avoid multiphoton dissociation.

In performing the TSLIF experiment we have observed significant photodecomposition in 7AI. The reaction product tends to form a film on the quartz windows of even the flow cells. A similar photolysis reaction has been observed by Zewail et al.[32] In addition, any metal surface that contacts with the 7AI solution catalyzes the thermal reaction of 7AI. In either case the reaction product gives rise to a fluorescence interference maximum at ∼400 nm upon excitation only by the 355-nm probe pulse. To solve this problem, we have developed a jet flow system in which the flow rate was controlled by a peristaltic pump (Cole-Parmer, Model 07520) and the jet nozzle was made of Pyrex glass so that no metal surface came in contact with the 7AI solution. Since the signal to noise ratio has been greatly enhanced due to the ultralow dark current and high detectivity of the ICCD, both pump and probe laser energies can be drastically reduced to further avoid the photochemical reaction of 7AI. With these improvements negligible photodecomposition of 7AI was observed throughout the TSLIF measurement.

Theoretical Calculation. Ab initio molecular orbital calculations were performed by using Gaussian 94 Rev D.3 programs. Geometry optimizations for all structures were carried out with the 6-31G* basis set at the Hartree−Fock (HF) level. This basis set has proven to be suitable for the dimer (or complex) formation incorporating hydrogen bonds.[47] Hessians, and hence vibrational frequencies, were also performed to check whether the optimized geometrical structures for those dimeric and complex forms are at an energy minimum, transition state, or higher order saddle point. The directly calculated zero-point vibrational energies (ZPE) were scaled by 0.9181[48] to account for the overestimation of vibrational frequencies at the HF level. Some special cases (see text) require a more advanced CBS-4 method,[40] which begins with a HF/3-21G(d) geometry optimization; the zero-point energy is computed at the same level. It then uses a large basis set (HF/6-311+G-(3d2f,2df,p) SCF calculation as a base energy and an MP2/6-31+G+ calculation with a CBS extrapolation to correct the energy through second order. The association energy, ΔH_{ac}, was calculated as the change in the total molecular enthalpy of formation for the conversion of the optimized monomer individually into the optimized dimer. A counterpoise correction procedure[49−51] has been applied to correct certain inconsistencies due to the basis-set superposition (BSSE). Hence, $\Delta H_{ac} = [H(\text{dimer or complex}) - 2H(\text{monomer}) - \Delta E_{cp}(\text{BSSE})]$, where ΔE_{cp}(BSSE) denotes the monomers energy corrected by the counterpoise correction procedure.

Results and Discussion

The following sections are organized according to a sequence of steps where we first performed detailed time-resolved spectral evolution of TSLIF to determine the rise and decay kinetics of the transient tautomer species. These in combination with theoretical approaches led us to propose a GSRPT mechanism followed by a derivation of the relaxation kinetics to rationalize the TSLIF experiment both qualitatively and quantitatively. Finally, on the basis of the proposed mechanism, attempts have also been made to rationalize the recent thermal-lensing experiment.[35]

Spectra and Dynamics of TSLIF. In Figure 2spectra a−t depict the time-resolved TSLIF spectra as a function of the delay time between pump and probe pulses in the range 300 ns to 200 μs. The spectral features of TSLIF were found to be time-evolution independent, consisting of an emission band maximum at 495 nm. In comparison to the proton-transfer emission obtained by only applying the 310-nm pulse excitation (see Figure 2, spectrum u), the TSLIF spectra not only are red shifted by ∼15 nm but also exhibit distinctly different spectral features. For example, a shoulder appearing at the onset region of the TSLIF is obscured in the prompt tautomer emission, which turns out to be crucial in interpreting the mechanism of GSRPT (vide infra). The results strongly indicate that the origin of the TSLIF is different from the prompt (i.e., non-time-resolved) proton-transfer emission which has been widely ascribed to the $(7AI(T))^*_2 \rightarrow (7AI(T))_2$ relaxation (see Figure 1). The insert of Figure 2 also depicts the integrated emission intensity versus various pump−probe delay times. The relaxation dynamics show

(43) (a) Cramer, C. J.; Truhlar, D. G. *J. Am. Chem. Soc.* **1993**, *115*, 8810. (b) Cramer, C. J.; Truhlar, D. G. *J. Comput. Chem.* **1992**, *13*, 1089.
(44) Hawkins, G. D.; Lynch, G. C. *QCPE* 606, 1995.
(45) Demas, J. N.; Crosby, G. A. *J. Phys. Chem.* **1971**, *75*, 991−1024.
(46) Chou, P. T.; Martinez, S. S. *Chem. Phys. Lett.* **1995**, *235*, 463.
(47) (a) Wang, J.; Boyd. R. J. *Chem. Phys. Lett.* **1996**, *259*, 647. (b) Wang, J.; Boyd, R. J. *J. Phys. Chem.* **1996**, *100*, 16141.
(48) Wong, M. W.; Wiberg, K. B.; Frisch, M. J. *J. Am. Chem. Soc.* **1992**, *114*, 1645.
(49) Stewart, J. J. P. *J. Comput. Chem.* **1989**, *10*, 221.
(50) Buemi, G. *THEOCHEM* **1988**, *41*, 379.
(51) Bliznyuk, A. A.; Voityuk, A. A. *THEOCHEM* **1983**, *41*, 343.

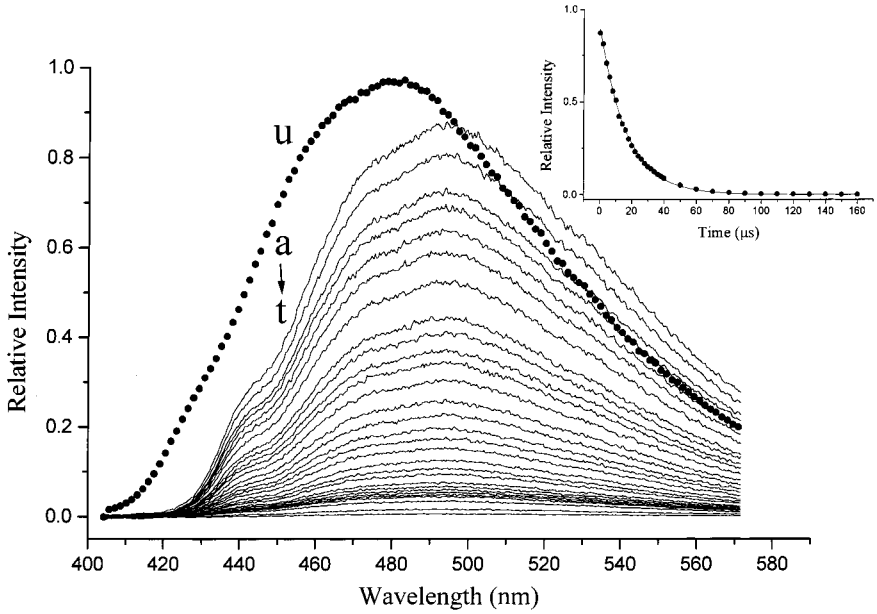

Figure 2. (—) Time-dependent spectral evolution of TSLIF. Spectra a−q: Each spectrum was obtained by an increment of 1.0 μs started from a delay time of 300 ns: r, 30 μs; s, 50 μs; t, 200 μs. Spectrum u: (···) the steady-state (i.e., only applying 310-nm pulse at zero delay time) tautomer emission of 7AI in *n*-heptane. In this study, 7AI was prepared to be 5.0×10^{-4} M in *n*-heptane and the solution was aerated to avoid the complication resulting from the triplet state. Insert: decay of TSLIF emission intensity by integrating the entire spectra as a function of the delay time.

Table 1. Spectral and Kinetic Data of GSRPT for 7AI in Various Solvents

solvent	η^a (cP)	steady-state fluorescence (λ_{max}, nm)	TSLIF (λ_{max}, nm)	$k_{obsd} \times 10^{-4}$ s^{-1} (298 K)	estd rise time (ns)[b]	activation energy (kcal/mol)
n-heptane	0.387	480	495	5.9	20	6.3 ± 0.3
cyclohexane	0.894	480	495	5.3	22	6.3 ± 0.5
dodecane	1.383	480	495	4.0	25	6.4 ± 0.3
n-hexadecane	3.032	481	497	3.0	25	6.6 ± 0.1

[a] *CRC Handbook of Chemistry and Physics*, 74th ed. 6−196, 197. [b] Data were taken by monitoring the time-dependent emission intensity at half of its maximum.

single-exponential decay behavior, and the decay rate was calculated to be $(5.9 \pm 0.2) \times 10^4$ s^{-1} in *n*-heptane.[52] Although our experimental results are qualitatively in agreement with those of previous reports,[33−35] several significant remarks should be pointed out. First of all, we have performed a series of power-dependent studies where the energy of either the pump or probe pulse was varied from 0.05 to 0.5 mJ with a large beam diameter of 3.5 and 3.0 mm for pump and probe pulses, respectively. The resulting TSLIF, being independent of the laser energy, always shows single-exponential decay behavior with a decay rate of $\sim 5.9 \times 10^4$ s^{-1} in *n*-heptane (see Table 1). The observed first-order decay kinetics of TSLIF are consistent with that reported by Suzuki et al. using transient absorption and thermal lensing techniques.[35] Conversely, Itoh et al. have applied a double-exponential function to fit their TSLIF decay traces[34] with a short (e.g., 17 μs in 3-methylpentane) and a long (47 μs) component attributed to 7AI(T) dimer and 7AI(T) monomer, respectively. Such a double-exponential decay behavior, however, was not observed in our low-power experiments. This discrepancy is believed to result from the difference in laser pulse energies as well as sample cuvette configuration used in the TSLIF experiment. In this study, when a higher power laser excitation (e.g., >5.0 mJ/pulse) was applied in a TSLIF experiment configured with a conventional nonflow sample cuvette, the yield of photoproduct was significant, giving rise to a non-negligible fluorescence background tailing down to 500 nm even excited by the probe pulse only. After a short period of accumulation, this background becomes very difficult to subtract, especially on the longer decay component where the TSLIF signal is even smaller than that of the background fluorescence. Note that in this study the interference resulting from photoproducts has been eliminated by the application of a jet flow configuration in combination with a low-power laser excitation (vide supra).

We have also carried out a series of experiments to measure the dynamics of TSLIF as a function of solvent viscosity from *n*-heptane ($\eta = 0.3$ cP) to hexadecane ($\eta = 3.03$ cP). Although the resulting TSLIF always exhibits single-exponential decay behavior, the decay rate seems to correlate with the viscosity which increases from 16.8 μs in *n*-heptane to 33 μs in hexadecane. A temperature-dependent study was also performed in various solvents.[53] The results showed significant temperature dependence. For example, in hexadecane, the lifetime of the transient species increased from 31.8 to 48.7 μs when the temperature decreased from 303 to 292 K (see Figure 3). A plot of the decay rate versus the reciprocal of temperature gave a sufficiently linear behavior (see insert of Figure 3), and accordingly, the activation energy and frequency factor were calculated to be 6.6 ± 0.2 kcal/mol and $(1.8 \pm 0.3) \times 10^9$ s^{-1}, respectively, in hexadecane. Table 1 lists the spectral and kinetic data of GSRPT for 7AI in various solvents. Interestingly, the activation energy, within experimental error, seems to be independent of hydrocarbon solvents used, of which the value is typically around 6.2−6.8 kcal/mol. The frequency factor of GSRPT is solvent-viscosity dependent, decreasing from 3.5×10^9 in *n*-heptane to 1.8×10^9 s^{-1} in hexadecane. In addition,

(52) We have carefully calibrated the flow rate to be ~1.0 mL/s. In a cylindrical flow system with a diameter of 1.0 mm in the cross section, we calculated that it requires ~1 ms to migrate 1 mm. Thus, the flow system applied in this study does not affect the observed relaxation dynamics within 1 ms.

(53) Due to the necessity of higher concentrations for preparing the 7AI dimer, which cause the crystallization of 7AI in the jet nozzle of the flow system, the temperature-dependent study was not performed at <10 °C. While at temperatures >40 °C, significant solvent vaporization takes place in this open flow system. In hexadecane, the temperature-dependent study was performed at >18 °C.

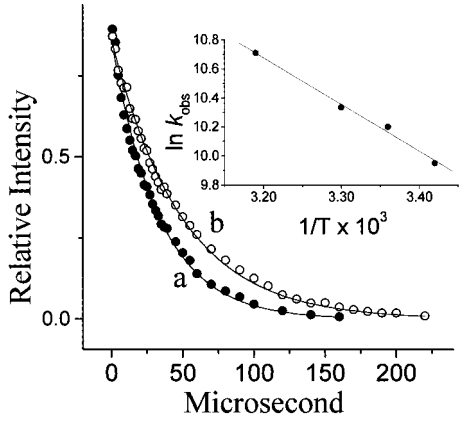

Figure 3. Temperature-dependent decay profile of TSLIF at (a) 303 and (b) 292 K in hexadecane. Insert: plot of the logarithm of the decay rate versus the reciprocal of temperature.

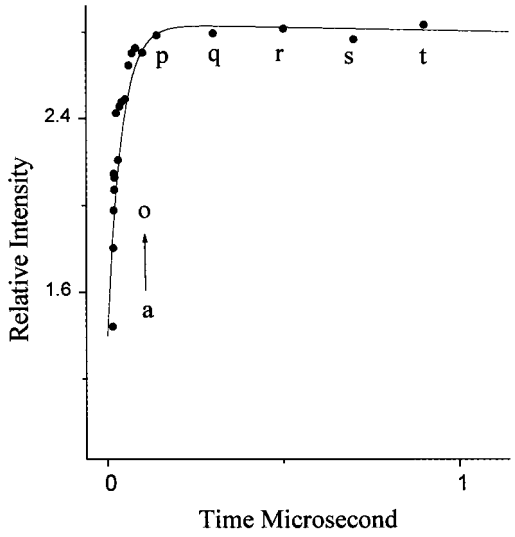

Figure 4. (●) Rise time of 7AI TSLIF emission intensity in *n*-heptane by integrating the entire spectra as a function of the delay time. Spectra a−o: Each data point was obtained by an increment of 5.0 ns started from a delay time of 15 ns; p, 150 ns; q, 300 ns; r, 500 ns; s, 700 ns; t, 850 ns. (—) Best least-squares-fitted curve for the rise time of the TSLIF using eqs 4−6, where parameters used for the curve fitting are described in the text.

the rate of GSRPT is deuterium-isotope dependent. In room-temperature *n*-heptane, the rate of GSRPT was measured to be 2.6×10^4 s^{-1} [54] in the deuterated 7AI dimer (D-7AI dimer) in comparison to that of 5.9×10^4 s^{-1} in the 7AI dimer. Consequently, through a temperature-dependent TSLIF study, an activation energy of GSRPT was estimated to be ~7.1 kcal/mol in the D-7AI dimer in *n*-heptane. Interestingly, the extracted frequency factor of 3.2×10^9 s^{-1} for GSRPT, within experimental error, is similar to that in the 7AI dimer.

Most importantly, comprehensive analyses reveal a previously unrecognized finite rise kinetics for the TSLIF. Figure 4 shows the TSLIF emission intensity in *n*-heptane as a function of the delay time within 100 ns. By monitoring the time-dependent emission intensity at half of its maximum a rise time of ~20 ns was roughly estimated in *n*-heptane. In addition, unlike the delay-time independence of the spectral features obtained at >100 ns (see Figure 2), the TSLIF tends to be red-shifted when the delay time decreases from 100 to 15 ns (see spectra b and a in Figure 5 for the comparison). Detailed analyses also indicate that except for changing the emission intensity, the rise dynamics of the TSLIF are found to be nearly independent of the added 7AI concentration and solvent viscosity as well as the laser intensity.

(54) This value was obtained under the presence of a small amount of undeuterated 7AI. The ^{1}H NMR and mass spectra gave isotopic purity of ~92%.

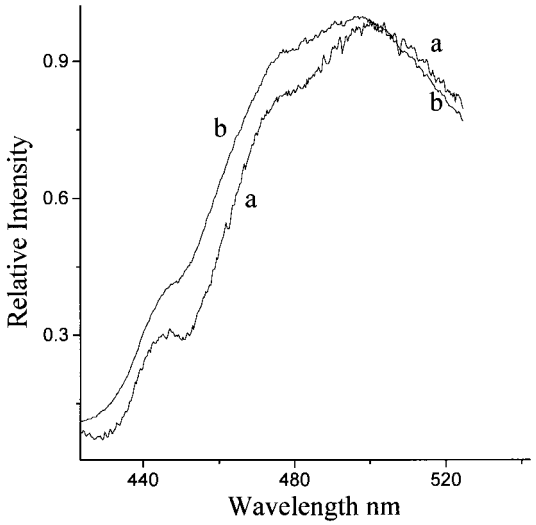

Figure 5. Time-dependent spectra of TSLIF obtained at a pump−probe delay time of (a) 15 and (b) 100 ns in *n*-heptane at 288 K.

Mechanisms of GSRPT. As concluded previously,[33−35] if the long-lived transient species were ascribed to the 7AI(T) dimer, the rise dynamics of TSLIF should be correlated with the decay rate of the prompt 7AI(T) dimer emission which was measured to be 3.3×10^8 s^{-1} ($\tau_f = 3.05$ ns) in *n*-heptane. For such a case, the rise dynamics of TSLIF could not be resolved due to the prevailing interference from the prompt proton-transfer emission. The finite, resolvable rise kinetics of TSLIF in combination with its distinctly different spectral features from the prompt 7AI(T) dimer emission lead us to conclude that the assignment of the slow transient component to a ground-state 7AI(T) dimer[33−35] may not be appropriate. Instead, an alternative and, in our opinion, more convincing interpretation is that the transient species originates from a minor dissociation channel of the excited 7AI(T) dimer during its life span, forming two 7AI(T) monomer species. Note that the excited 7AI(T) dimer (i.e., $(7AI(T))_2$*) is produced through an ultrafast ESDPT of the 7AI(N) dimer (i.e., $(7AI(N))_2$).[27−32] Since there is no initial population of the 7AI(T)* monomer, the Le Chatelier's principle simply predicts that a shift in equilibrium toward the dissociation of $(7AI(T))_2$*), forming 7AI(T) monomers, may occur within the life span of $(7AI(T))_2$*. Whether the dissociation is adiabatic or nonadiabatic as well as the branching ratio to form 7AI(T) will be discussed in the subsequent section.

The escaped 7AI(T) monomer may undergo three possible deactivation (i.e., reverse proton transfer) pathways depicted in Scheme 1 to regenerate 7AI(N) in the ground state. Process 1 incorporates an intramolecular proton-transfer reaction of the

Scheme 1

$$7AI(T) \xrightarrow{k_{pt1}} 7AI(N) \quad (1)$$

$$7AI(T) + 7AI(T) \underset{k_{-TT}}{\overset{k_{TT}}{\rightleftharpoons}} (7AI(T))_2 \xrightarrow{k_{pt2}} 7AI(N) + 7AI(N) \quad (2)$$

$$7AI(T) + 7AI(N) \underset{k_{-TN}}{\overset{k_{TN}}{\rightleftharpoons}} 7AI(T)/7AI(N) \xrightarrow{k_{pt3}} 7AI(N) + 7AI(N) \quad (3)$$

7AI(T) monomer. In the gas phase, the activation energy of the reaction 7AI(N) → 7AI(T) has been estimated to be ~60 kcal/mol by an ab initio approach.[55] Since 7AI(T) was calculated to be ~14 kcal/mol higher in energy than that of 7AI(N),[21,41,55] the activation energy for the GSRPT of 7AI(T) is then calculated to be ~46 kcal/mol. We have also performed a calculation for the GSRPT of the 7AI(T) monomer in solution based on the isodensity polarized continuum model (IPCM)[56] and estimated the activation energy to be 44.5 kcal/mol in *n*-heptane, indicating that the perturbation from a solvent induce-dipole interaction is rather small for the intramolecular GSRPT. Such a high activation energy may be rationalized by a four-member-ring proton-transfer system like 7AI(T) in which the proton migration has to encompass an enormously large strain energy. Accordingly, the rate of intramolecular proton transfer in the 7AI(T) monomer, k_{pt1}, should be exceedingly small and may not play a key role for the observed relaxation dynamics.

Alternatively, the 7AI(T) monomer may undergo two other possible relaxation pathways. First, it may recombine with another 7AI(T) to form a 7AI(T) dimer followed by reverse double proton transfer with a rate of k_{pt2} (process 2). In this study, the concentration of 7AI(N) dimer was generally prepared to be within $(1.0-5.0) \times 10^{-4}$ M in the ground state. Applying a moderately low power excitation (0.5 mJ/pulse) and assuming a 100% efficiency for the ESDPT, we estimated the production of $(7AI(T))_2^*$ to be $<3 \times 10^{-6}$ M.[57] Thus, the 7AI(T) monomer generated from a minor dissociation channel of $(7AI(T))_2^*$ should be much less than 3.0×10^{-6} M. Taking a diffusion-controlled recombination rate constant as an upper limit ($\sim 2.0 \times 10^{10}$ M^{-1} s^{-1} in *n*-heptane), the association rate of 7AI(T) forming 7AI(T) dimer was calculated to be $<10^4$ s^{-1} (i.e., a rise time of >100 μs), which is apparently too slow to account for the experimentally observed ~15−20 μs life-span transient species with a rise component of tens of nanoseconds. Therefore, it is more plausible to propose that the reverse proton transfer of 7AI(T) takes place through the catalysis of 7AI(N) by forming a 7AI(T)/7AI(N) hydrogen-bonded complex (process 3). Similar to that discussed in process 2, the rise kinetics in process 3 should correlate with a bimolecular process associated with 7AI(N) concentration. Since [7AI(N)] prepared in this study ($>10^{-4}$ M) is much greater than that of 7AI(T) ($\ll 10^{-6}$ M) the rise kinetics of TSLIF should correlate with k_{TN} [7AI(N)] based on a pseudo-first-order approximation. In other words, the TSLIF rise kinetics may depend on [7AI(N)] and/or solvent viscosity if k_{TN} is limited by a diffusion-controlled process. Such a derivation however contradicts the experimental results which conclude both concentration and viscosity independence for the rise kinetics of TSLIF. Kinetically, a possible solution is to incorporate a reverse dissociation pathway of 7AI(T)/7AI(N) → 7AI(T) + 7AI(N) with a rate constant of k_{-TN} (see Scheme 1). This assumption is very reasonable if one considers the similar association reaction 7AI(N) + 7AI(N) ⇌ $(7AI(N))_2$, in which an equilibrium constant has been determined to be 1.8×10^3 M^{-1} in cyclohexane.[3,39]

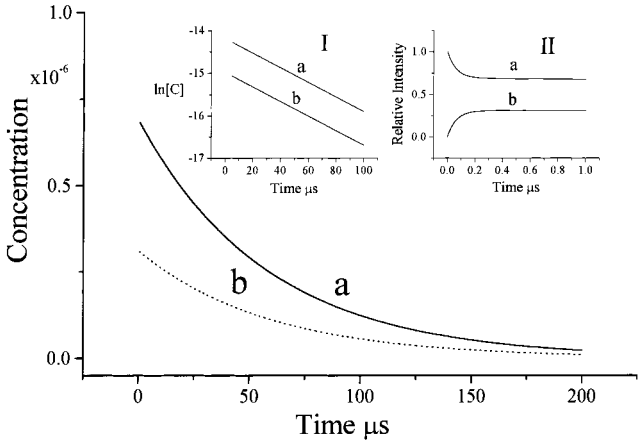

Figure 6. Computer simulation of the relaxation dynamics of (a) 7AI(T) and (b) 7AI(T)/7AI(N) complex using eqs 4 and 5, respectively, at >100 ns. The initial [7AI(T)] was taken to be 1.0×10^{-6} M. See text for parameters used in the simulation. Insert I: logarithm of time-dependent 7AI(T) and 7AI(T)/7AI(N) at >100 ns. Insert II: time-dependent 7AI(T) and 7AI(T)/7AI(N) within 0 to 1.0 μs.

On the basis of a coupled reaction incorporating processes 1 and 3, the relaxation dynamics of 7AI(T) and 7AI(T)/7AI(N) can be expressed in eqs 4 and 5, respectively

$$[7AI(T)] = \frac{[7AI(T)]_0}{\lambda_2 - \lambda_1}\{(\lambda_2 - x)e^{-\lambda_1 t} + (x - \lambda_1)e^{-\lambda_2 t}\} \quad (4)$$

$$[7AI(T)/7AI(N)] = \frac{k_{TN}[7AI(N)][7AI(T)]_0}{\lambda_2 - \lambda_1}\{e^{-\lambda_1 t} - e^{-\lambda_2 t}\} \quad (5)$$

where

$$\lambda_{1,2} = {}^1/_2[(x + y) \mp \{(x - y)^2 + 4k_{-TN}k_{TN}[7AI(N)]\}^{1/2}]$$

$$x = k_{pt1} + k_{TN}[7AI(N)]; \quad y = k_{pt3} + k_{-TN}$$

Note that k_{pt1} is $\ll k_{pt3}$ according to the previous discussion and can thus be neglected for further derivation. Here, we take the hydrogen-bonding formation rate constant k_{TN} to be a diffusion-controlled limit, which is $\sim 2.0 \times 10^{10}$ M^{-1} s^{-1} in *n*-heptane. k_{TN}/k_{-TN} is equivalent to the equilibrium constant K_{eq} for the formation of a 7AI(T)/7AI(N) complex. Assuming that the 7AI(T)/7AI(N) complex possesses similar hydrogen-bonding strength as the 7AI(N) dimer and hence the same K_{eq} of $\sim 1.8 \times 10^3$ M^{-1}, k_{-TN} was deduced to be 1.1×10^7 s^{-1}. k_{pt3} should correlate with the decay dynamics of TSLIF and thus is taken to be 5.9×10^4 s^{-1} in *n*-heptane. Accordingly, a computer simulation generated by plugging the aforementioned parameters for eqs 4 and 5 is shown in Figure 6. The result clearly indicates that both 7AI(T) and 7AI(T)/7AI(N) exhibit identical decay kinetics at a delay time of >100 ns, while a fast decay and rise within 100 ns was observed for 7AI(N) monomer and 7AI(T)/7AI(N) complex, respectively. In fact, since k_{-TN} is generally greater than the pseudo-first-order formation rate, k_{TN} [7AI(N)], the rise kinetics observed in the 7AI(T)/7AI(N) complex essentially corresponds to the decay of the 7AI(T)/7AI(N) complex. The results account for the nearly 7AI(N) concentration and solvent-viscosity independence of the TSLIF rise component. Note that the derivation is based on the instant population of the 7AI(T) monomer at $t = 0$. In a real case the population of 7AI(T) should possess a rise time of 3.05 ns which is equivalent to the decay rate of $(7AI(T))^*_2$) in *n*-heptane.

(55) Gordon, M. S. *J. Phys. Chem.* **1996**, *100*, 3974.

(56) (a) Greenwood, J. R.; Capper, H. R.; Allan, R. D.; Johnston, G. A. R. *THEOCHEM* **1997**, *419*, 97. (b) Gonzalez, C.; Restrepo-Cossiot, A.; Márquez, M.; Wiberg, K. B.; De Rosa, M. *J. Phys. Chem. A.* **1998**, *102*, 2732. In this study, the transition state was calculated by a MP2/6-31G** basis set in the gas state. The resulting structure was then used to perform the IPCM calculation to obtain the activation energy in solution.

(57) An absorbance of ~0.5 for the 7AI(N) dimer at 310 nm was applied in this study. This in combination with a 3.5-mm diameter, 0.5-mJ laser pulse gives an estimated value of 3×10^{-6} M for $(7AI(T))_2^*$ originally produced from the ESDPT of $(7AI(N))_2^*$.

(58) pK_a of the N_1H^+ proton in 7AI(T) is taken to be the same as that of the protonated 7-methylazaindole.[17]

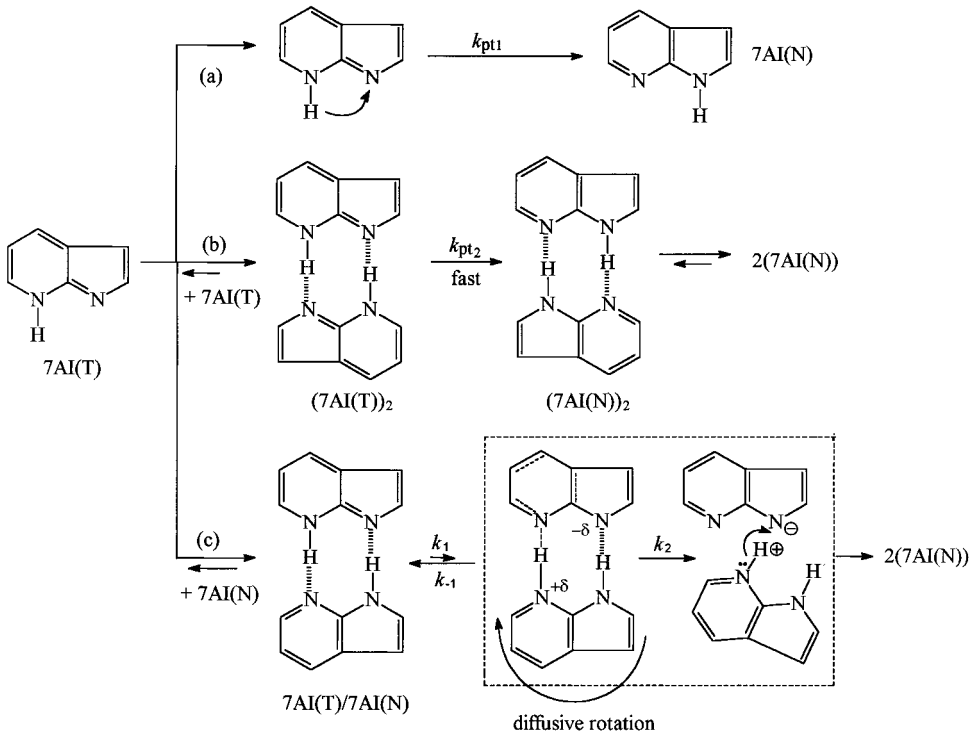

Figure 7. Proposed reverse proton-transfer mechanisms of 7AI(T) in the ground state.

The observed time-dependent TSLIF should be the sum of the relaxation dynamics for 7AI(T) and 7AI, i.e., the combination of eqs 4 and 5. Unfortunately, at this stage, we are not able to extract the intensity ratio without knowing the fluorescence yield and the absorption cross section at 355 nm, ϵ_{355}, for both 7AI(T) and 7AI(T)/7AI(N). These unknown parameters make it unfeasible to use eqs 4 and 5 to fit the experimental results. Nevertheless, an attempt has been made by using eq 6 expressed as

$$\alpha[7AI(T)]_t + \beta[7AI(T)/7AI(N)]_t \qquad (6)$$

where α and β are factors incorporating fluorescence yield and ϵ_{355} for 7AI(T) and 7AI(T)/7AI(N), respectively, to fit the experimental result shown in Figure 4. The time-resolved $[7AI(T)]_t$ and $[7AI(T)/7AI(N)]_t$ were derived from eqs 4 and 5, in which all the parameters except for k_{-TN} are taken to be the same as those used to obtain Figure 6. A best fit by varying k_{-TN}, α, and β to Figure 4 gives rise to β/α and k_{-TN} of 5.8 and 1.7×10^7 s^{-1}, respectively (see Figure 4, solid line). In addition, the analysis also indicates that so far as $k_{-TN} \gg k_{TN}$-[7AI(N)], the rise dynamics of TSLIF are nearly independent of [7AI(N)] because the rise kinetics of 7AI(T)/7AI(N) essentially correspond to the dissociation rate, k_{-TN}, of the 7AI(T)/7AI(N) complex. Although this result may not have too much significance due to the fixed relaxation rate (k_{pt3}) and bimolecular rate (k_{TN}) constants, it definitively indicates that by adjusting certain parameters the experimental results can be rationalized by a combination of relaxation processes 1 and 3. Finally, it should be noted that the process of 7AI(T) dimer → 7AI(N) dimer reverse proton transfer is nevertheless the major relaxation channel. However, it is proposed that, similar to the ultrafast ESDPT in the 7AI dimer,[30−32] the ground-state 7AI(T) dimer, once formed with pre-existing intact dual hydrogen bonds, should also undergo a rapid reverse proton-transfer reaction. For this case the rate-determining step in an overall proton-transfer cycle is limited by the decay of $(7AI(T))^*_2$ emission, which is $\sim 3.33. \times 10^8$ s^{-1} ($\tau \sim 3.0$ ns) in *n*-heptane.

The structure of the 7AI(T)/7AI(N) complex is intriguing and is crucial to interpret the GSRPT of 7AI. A possible hydrogen-bonding configuration incorporating a cyclic dual hydrogen-bonding formation is depicted in Figure 7, which exhibits a global minimum calculated by a 6-31G** basis set. The hydrogen-bonding strength, taking the value of ΔH_{ac} for the association (see the Experimental Section), was calculated to be −14.3 kcal/mol, which is even stronger than that of −11.3 kcal/mol calculated for the 7AI(N) dimer.[39] Hence, the formation of a 7AI(T)/7AI(N) hydrogen-bonding complex is theoretically predictable, supporting its existence concluded in the experimental results. However, if the reverse proton transfer takes place via the cooperative double proton migration, the same product, i.e., the 7AI(T)/7AI(N) complex, should be produced, which would not influence the observed TSLIF dynamics. Alternatively, we tentatively propose the ground-state reverse proton-transfer mechanism depicted in Figure 7, process c, where the first-step proton transfer may occur via the deprotonation of the 7AI(T)/7AI(N) complex. This step is proposed to be endergonic, forming an active complex or intermediate-like ion pair in which the partial positive charge of the pyridinal nitrogen in 7AI(N) and a build-up of partial negative charge density at the pyrrole site of 7AI(T) create an electrostatic attraction. This acts as a driving force for the geometry adjustment (e.g., the rotational diffusion) between 7AI(T) and 7AI(N) to a right conformation so that the second-step proton transfer can take place through a lowest potential energy surface. For this case, 7AI(N) acts as a proton donor and acceptor simultaneously to achieve an autocatalytic process. Kinetically, if the rate of back proton transfer k_{-1} (see process c in Figure 7) is much faster than the rate of large-amplitude rotational diffusion, k_2, while both k_{-1} and k_2 are $\gg k_1$, the overall rate of the reverse proton transfer k_{pt3} in process c can be expressed as

$$k_{pt3} = k_2\left(\frac{k_{-1}}{k_1}\right) = k_2 e^{-\Delta G/RT}$$

where ΔG is the energy difference between 7AI(T)/7AI(N) and

its associated ion pair in process c. This kinetic expression qualitatively explains the measured nearly solvent-viscosity-independent but isotope-dependent activation energy for GSRPT, while the difference in the decay rate in various viscous solvents is mainly due to the different frequency factor associated with the viscosity-dependent large-amplitude diffusive migration. Note that such a proposed GSRPT mechanism is quite different from that of ESDPT in the 7AI(N) dimer in which the global potential energy surface, to a certain extent, may correlate with the cooperative motion of the dual hydrogen bonds, resulting in a very small energy barrier. Consequently, the rate of ESDPT in 7AI(N) dimer is mainly governed by a tunneling mechanism.

Another intriguing question regards whether the deprotonation in the 7AI(T)/7AI(N) complex originates from the pyrrolyl proton in 7AI(N) (i.e., N_1H) or the pyridinal proton (N_7H) in the 7AI(T) part. A qualitative answer to this query may be given by the difference in the acid/base property of various functional groups in the complex. For the N_1H proton in 7AI(N) the pK_a value of 12.1 is a weaker acid than that of the N_1H^+ site (pK_a = 8.9) in 7AI(T). Therefore, the first step initiated by the deprotonation of 7AI(N) seems to be thermodynamically more unfavorable than the deprotonation taking place through the 7AI(T) moiety, although we have no direct evidence at this stage to support this viewpoint due to the lack of pK_a data for the N_7H site in 7AI(T).

Interpretation of the Thermal-Lensing Experiment. This proposed GSRPT mechanism also rationalizes several previously unsolved controversies. First of all, upon excitation by the probe pulse, the emission spectral features of 7AI(T) and/or 7AI(T)/7AI(N) are expected to be different from those of the 7AI(T) dimer due to the different hydrogen-bonding strength, rationalizing the TSLIF results shown in Figures 2 and 5. In addition, the spectral difference between 7AI(T) and 7AI(T)/7AI(N) can only be partially distinguished by the rise component, while the decay kinetics for both are identical. More importantly, the proposed mechanism renders a rational interpretation for the thermal lensing experiment.[35] We took the results of the thermal lensing experiment performed by Suzuki et al., concluding that

$$\frac{U_S}{U_T} = \frac{\varphi_r \Delta H}{\alpha E_{ex}} = 0.012 \qquad (7)$$

where E_{ex} is the energy of excitation which corresponds to a 320-nm (31 250 cm^{-1}) laser pulse used by Suzuki et al.,[35] U_T is proportional to the total heat dissipated in a proton-transfer cycle, U_S corresponds to the amount of heat dissipation associated with the slow component, α is the fraction of energy released as heat against the total energy absorbed, and ΔH represents the enthalpy change between 7AI(T) and 7AI(N) dimers in the ground state. Finally, ϕ_r denotes the reaction yield to produce the long-lived transient species, which has previously been assumed to be unity due to the ultrafast ESDPT. However, according to our proposed mechanism, ϕ_r can no longer be unity but rather the fraction of dissociation of the 7AI(T) dimer in the excited state, forming the 7AI(T) monomer. Although ϕ_r is experimentally inaccessible at this stage, it can be estimated by a simple approach where α and ΔH are taken to be 0.90[35] and 24 kcal/mol (an average value calculated in ref 38 and this study), respectively. Plugging these parameters into eq 7, a ϕ_r value of 0.04 is deduced. Note that, if the dissociation of $(7AI(T))^*_2$ is nonadiabatic, giving rise to two ground-state 7AI(T) monomer species, this process can be treated as another radiationless quenching pathway of $(7AI(T))^*_2$. For the case of an adiabatic process, the dissociation results in an excited 7AI(T) monomer species which may undergo different relaxation dynamics from $(7AI(T))^*_2$. However, such a small fraction of 7AI(T) may not be resolved from the fluorescence decay dynamics since its relaxation dynamics (e.g., 2.1 ns reported in 3-methylpentane[34]) are only slightly different from those of the 7AI(T) dimer (3.0 ns). Consequently, a single-exponential lifetime of the prompt tautomer emission has been reported in many places as well as in this study. At this stage, whether the dissociation is an adiabatic or nonadiabatic process unfortunately cannot be determined.

Conclusion

Comprehensive analyses of the ground-state reverse proton transfer in 7AI reveal the following significant remarks:

(i) The ground-state transient tautomer species undergoes single-exponential decay dynamics, which upon second laser excitation exhibits a fluorescence with the peak maximum ~15-nm red shifted with respect to the steady-state tautomer (i.e., (7AI(T) dimer) emission.

(ii) A previously unrecognized finite rise time (~20 ns, depending on solvents) for the TSLIF was observed. The TSLIF spectrum obtained at the rise component is different from that of the decay component.

(iii) The decay dynamics of TSLIF are dependent on the solvent viscosity, which mainly affects the frequency factor of the reverse proton transfer.

The results lead us to conclude that the ground-state transient species originates from the monomer of 7AI proton-transfer tautomer (7AI(T)) produced by a minor dissociation channel (~4%) of the excited 7AI(T) dimer, which subsequently undergoes a slow reverse proton transfer via the formation of a 7AI(T)/7AI(N) hydrogen-bonded complex. This proposed mechanism rationalizes the recent thermal lensing experiment which concluded that the 7AI(T) dimer is only 0.97 kcal/mol higher in energy than the 7AI(N) dimer,[35] while theoretical approaches in this study as well as previous reports,[38,39] in contrast, predict an energy difference of >20 kcal/mol.

The GSRPT was also investigated for 7AI/methanol and/or 7AI/acetic acid hydrogen-bonded complexes. However, the long-lived transient species was not observed by either transient absorption or TSLIF experiments. For the case of 7AI/acetic acid complex, the association constant is at least 1 order of the magnitude larger than that of the 7AI dimer.[39] Assuming similar hydrogen-bonding strength in the excited state, the fraction of dissociation for the 7AI(T)*/ACID complex, forming 7AI(T), is then expected to be much less than 4% and hence may not be detectable. In methanol solution, 7AI(T) produced from the dissociation of the 1:1 7AI(T)*/methanol complex will be immediately solvated, forming a 7AI(T)/methanol complex which, similar to that of the methanol-assisted ESDPT,[6−13] is believed to undergo a fast GSRPT. For this case the rate of the overall proton-transfer cycle should be limited by the decay of the 7AI(T)*/methanol complex.

Acknowledgment. This work was supported by the National Science Council, Taiwan, ROC (Grant No. NSC 87-2119-M-194-002).

JA982940D